The irradiated brain microenvironment supports glioma stemness and survival via astrocyte-derived Transglutaminase 2

Tracy J. Berg[1], Carolina Marques[2], Vasiliki Pantazopoulou[1], Elinn Johansson[1], Kristoffer von Stedingk[3,4], David Lindgren[1], Elin J. Pietras[5], Tobias Bergström[6], Fredrik J. Swartling[6], Håkan Axelson[1], Massimo Squatrito[2], and Alexander Pietras[1]

[1]Division of Translational Cancer Research, Department of Laboratory Medicine, Lund University, Lund, Sweden [2]Seve Ballesteros Foundation Brain Tumor group, CNIO, Madrid, Spain [3]Department of Pediatrics, Clinical Sciences Lund, Lund University, Lund, Sweden [4]Department of Oncogenomics, M1-131 Academic Medical Center University of Amsterdam, Amsterdam, Netherlands [5]Biotech Research and Innovation Centre, University of Copenhagen, Copenhagen 2200, Denmark [6]Department of Immunology, Genetics and Pathology, Science for Life Laboratory, Uppsala University, 751 85 Uppsala, Sweden

Correspondance: Alexander.Pietras@med.lu.se , +46709928629

1

Abstract

The tumor microenvironment plays an essential role in supporting glioma stemness and radioresistance; however, little is known about how the microenvironment responds to radiation. Here, we found that astrocytes, when pre-irradiated, increased stemness and survival of co-cultured glioma cells. Tumor-naïve brains increased reactive astrocytes in response to radiation, and mice subjected to radiation prior to implantation of glioma cells developed more aggressive tumors. We identified extracellular matrix derived from irradiated astrocytes as a major driver of this phenotype, and astrocyte-derived transglutaminase 2 (TGM2) as a promoter of glioma stemness and radioresistance. TGM2 inhibitors abrogated glioma stemness induced by irradiated astrocytes. TGM2 inhibition reduced survival of glioma cells in *in vitro* and *ex vivo* tumor models. These data suggest that irradiation of the brain results in the formation of a tumor-supportive microenvironment. Therapeutic targeting of radiation-induced, astrocyte-derived extracellular matrix proteins may enhance the efficacy of standard of care radiotherapy in glioma.

Introduction

Glioblastoma multiforme (GBM) is the highest grade glioma, with less than a 10% five year survival rate.[1] GBM is typically treated by surgical resection, followed by radiation and chemotherapy, yet nearly all tumors recur after treatment.[2] Tumors which recur generally form within or overlapping the original tumor volume[3] and within the initial field receiving high-dose radiation, suggesting that the recurring tumor forms within the irradiated brain microenvironment. The recurred tumors have limited treatment options, and the mechanisms underlying therapeutic resistance are incompletely understood.

Recurrence of GBM is often attributed to radioresistant glioma cells. The radioresistant tumor cell phenotype appears to be closely related to the concept of tumor stemness, in that tumor cells surviving radiotherapy display several characteristics of stem cells, such as enhanced self-renewal and increased drug efflux capabilities, as compared to sensitive tumor cells.[4,5] Understanding which factors promote stemness and treatment resistance of glioma cells is of intense interest in developing new therapies in glioma. A large number of studies over the past decade have established that there is considerable plasticity in glioblastoma cell phenotypes,[6-11] that stem cell characteristics can be acquired by non-stem-like cells,[8,9,12-15] and that microenvironmental cues such as hypoxia,[16] extracellular matrix proteins,[17-25] or growth factors secreted by stromal cells[26-28] may be sufficient to induce tumor cell stemness and therapeutic resistance. The role of the microenvironment in regulating tumor stemness is further supported by the finding that stem-like tumor cells are enriched in specific tumor niches; in GBM, primarily the perivascular niche (PVN) and hypoxic compartments.[16,29,30]

The variety of stromal cell types found in the GBM microenvironment include cells associated with the PVN and hypoxic compartments, such as astrocytes, microglia, endothelial cells, and pericytes.[31] Several of these cell types have been shown to actively contribute to glioma aggressiveness.[32,33] Little is known about how these cells respond to radiotherapy, and how they in turn might affect the associated glioma cells after irradiation. We sought to determine whether irradiation of the brain tumor microenvironment might affect the phenotype and therapeutic response of glioma cells. We identified astrocyte-derived transglutaminase 2 as a potential radiation-induced modifier of the tumor microenvironment, which protected against radiation-induced glioma cell death, and may thus serve as a potential therapeutic target in GBM.

Results

Irradiated astrocytes promote glioma cell stemness

We devised a co-culture scheme with which we could rapidly test a variety of control or irradiated stromal cells for their ability to increase one of the indicators of stemness in glioma cells, the side population (SP). [34-37] To do this, we pre-irradiated four stromal cell types before co-culturing with non-irradiated PDGFB-induced glioma primary cells (PIGPC) derived from RCAS-*PDGFB*-induced gliomas in *Nestin-tv-a Ink4a/Arf*^{-/-} mice. Non-irradiated PIGPC were added to the pre-irradiated cells for co-culture for 48 h, followed by an SP assay. The experimental design for this screening is outlined in Figure 1A.

We pre-treated mouse brain endothelial cells (BEND3; Fig 1B), human microglia (HMC3; Fig 1C), primary human brain vascular pericytes (HBVP; Fig 1D), and primary human astrocytes (Fig 1E) with either 0 Gy or 10 Gy radiation, which is a therapeutic radiation dose in our tumor models. PIGPC were used as control, non-stromal cells in each experiment to determine if co-culture with irradiated tumor cells alone could promote stemness features and to control for cell density. Only co-culture with pre-irradiated astrocytes stimulated a marked and consistent increase in SP of the PIGPC cells (Fig 1E). This suggests that irradiated astrocytes support glioma cell stemness.

To rule out that the stromal cells alone might contribute to the SP, we measured the SP of all the cell types before and after irradiation. Neither BEND3, HBVP, HMC3, nor astrocytes alone had a consistent SP before irradiation (Supplemental Fig 1). Irradiation did not produce an SP of these stromal cells except in the case of HMC3, in which an erratic increase in SP was detected, which did not result in a statistically significant difference from non-irradiated cells (Supplemental Fig 1). Co-culture of PIGPC with irradiated PIGPC also did not result in a significant increase in SP in any of the co-culture assays (Fig 1B-E).

Finding that tumor-naïve astrocytes irradiated in culture can promote the SP of glioma cells, we sought to determine whether astrocytes in the tumor-naïve brain might show increases in activation in response to irradiation. We stained brains from mice treated with 0 Gy or 10 Gy of radiation for GFAP, one of the markers of activation, and identified a trend of increased GFAP in the brains of mice treated with radiation (Fig 1F-H). This is consistent with previous findings from Chiang et al, [38] who showed increased GFAP expression 120-180 days post irradiation with 25-40 Gy dose of radiation.[38,39]

5

The irradiated brain microenvironment supports tumor growth

After finding that pre-irradiated astrocytes could promote stemness features of glioma cells, we sought to determine whether radiation-induced changes in the brain microenvironment influence tumor growth or development. We therefore pre-irradiated mice with either 0 Gy or 10 Gy radiation to the brain, followed by intracranial injection with PIGPC 72 h post-radiation. Mice were sacrificed upon development of brain tumor symptoms (Fig 2A). Mice which were pre-irradiated developed tumors with increased microvascular proliferation (Fig 2B-D) and increased Ki67 positive nuclei (Fig 2E-F), both indicators of more aggressive, high grade glioma. Astrocytes were abundant within the tumor and associated with sites of microvascular proliferation (Fig 2G), one well established site enriched with stem-like glioma cells.[29] These findings suggest that irradiation of the brain microenvironment supports tumor growth and that astrocytes may play a role in this process.

Irradiated astrocytes produce a modified extracellular matrix which supports glioma cell stemness and radiation resistance

Co-culture of astrocytes with glioma cells may increase the glioma cell SP through direct cell-cell contact, secretion of soluble factors, or through modification of the extracellular matrix (ECM). We devised two assays to isolate the effects of soluble factors and ECM components from irradiated astrocytes on glioma cells (Fig 3A). To determine whether pre-irradiated astrocytes stimulated increased SP of PIGPC via soluble factors, we suspended astrocytes in sodium alginate beads followed by treatment with either 0 Gy or 10 Gy irradiation. We then co-cultured these suspended astrocytes with PIGPC adhered to culture dishes, allowing the astrocytes to secrete cytokines into the media without direct cell-cell contact with PIGPC. We did not detect an increase

6

in SP of PIGPC cells cultured in conditioned media from pre-irradiated astrocytes suspended in alginate beads (Supplemental Figure 2). This suggested the possibility of insoluble factors influencing the SP of the PIGPC cells. We therefore tested the potential of matrix proteins to affect the SP of PIGPC cells.

To generate purified ECM from astrocytes, confluent astrocytes were treated with either 0 Gy or 10 Gy radiation, then cultured for 10 days. The plates were de-cellularized, leaving behind insoluble matrix proteins (astrocyte derived matrix, ADM). Glioma cells were cultured on matrix from either 10 Gy-irradiated astrocytes (ADMi) or control, 0 Gy-treated astrocytes (ADMc) to examine the influence of ADM in various assays measuring stemness and radiation resistance (Fig 3A). Those assays include SP, self-renewal, and survival after irradiation.

Both PIGPC (Fig 3B) and the serum-free cultured human glioma cell line U3082 (Fig 3C) showed increased SP when cultured on ADMi. This suggests that changes in astrocyte derived matrix proteins after irradiation may be responsible for the increased SP of glioma cells co-cultured with irradiated astrocytes (Fig 1E). Another important measure of stemness is self-renewal capabilities, which can be measured by sphere formation capacity of clonal densities of glioma cells. To determine whether ADMi affected self-renewal, U3082 cells were conditioned by culturing for 5 days on ADMc or ADMi, followed by plating at clonal densities in 6-well dishes. After initial sphere formation, the spheres were disrupted and single cells were replated at clonal densities. There were no changes in formation of primary spheres (Fig 3D), however quantification of secondary spheres revealed increased sphere formation of cells cultured on ADMi compared to ADMc (Fig 3D). Combined, the increase in SP and self-renewal of glioma cells cultured on ADMi

compared to those cultured on ADMc suggests that astrocytes modify the ECM after irradiation to support glioma cell stemness.

To determine whether ADMi promotes radiation resistance of glioma cells, we plated clonal densities of human glioma U251 cells on ADMc or ADMi, followed by irradiation at 4 Gy, a dose that reduced colony formation by approximately 50% (Fig 3E). Glioma cells cultured on ADMi showed increased colony formation after irradiation compared to cells cultured on ADMc (Fig 3E). This suggests that matrix from irradiated astrocytes has the capacity to promote radiation resistance of glioma cells.

RNA sequencing of U3082 cells cultured on ADMc or ADMi for 48 h revealed that culture on ADMi indeed resulted in global gene expression changes of glioma cells. Among gene sets significantly upregulated after culture on ADMi were pathways associated with the extracellular matrix, basement membrane, and integrin signaling (Fig 3F). Notable gene sets among the downregulated ones were associated with translation initiation and oxidative phosphorylation (Fig 3F).

Taken together, these data suggest that astrocytes modify matrix proteins after irradiation in a manner which promotes stemness, including radiation resistance of glioma cells.

Irradiation induces a reactive astrocyte phenotype which persists within the original tumor volume after irradiation

Astrocytes are an abundant cell type in the brain and in gliomas and are likely to survive radiotherapy.[40] It is well established that astrocytes respond to damage to the brain,[41] including radiation,[38,39] and that this response typically involves a process termed reactive gliosis. This response varies across regions of the brain and damage type; however some phenotypes are shared amongst most reactive astrocytes,[41] such as GFAP upregulation and morphological reorganization, two hallmarks of reactive gliosis.[41]

To understand the response of astrocytes to radiation in our models, we examined astrocytes after a 10 Gy dose of radiation in normal and tumor-bearing brains as well as purified, primary human astrocytes. Tumors were generated in *Nestin-tv-a Ink4a/Arf^{-/-}* mice by injection with RCAS-*PDGFB* and were irradiated upon symptoms of brain tumor with either 0 Gy or 10 Gy, then sacrificed 72 h later (Fig 4A). Whole brain sections were stained for Olig2 (green), which marks glioma cells, and GFAP (red), which marks activated astrocytes (Fig 4B-C). In 0 Gy-treated tumor-bearing brains, reactive astrocytes are enriched at the tumor borders and are found throughout the tumor itself, as can be seen in scans of the whole brain sections in Figure 4B. Tumor area is demarcated with a white line. Closer examination reveals astrocytes found within stromal compartments (white arrow in high-magnification, merged image) and amongst the Olig2-positive glioma cells (blue arrow) (Fig 4B).

After irradiation, Olig2-positive cells decrease to nearly undetectable levels; however, GFAP staining is retained in areas of the likely original tumor volume (Fig 4C, likely tumor volume

9

bounded in white identified by GFAP staining). In the areas demarcated by strong GFAP staining (white borders), this results in an increased ratio of GFAP to Olig2 in irradiated brains compared to untreated brains (Fig 4D).

In addition to characterizing astrocytes *in vivo*, we sought to characterize the *in vitro* response of astrocytes to radiation. Because *in vitro* cultivation of primary astrocytes shifts them to a more reactive phenotype than seen *in vivo*,[42] we tested whether our primary cultured astrocytes underwent any features of reactive gliosis in culture. Astrocytes exposed to 10 Gy radiation developed the classic morphology of somatic hypertrophy (Fig 4E) and expressed elevated levels of the reactive marker vimentin (Fig 4F).[42] Furthermore, irradiated astrocytes expressed increased levels of the soluble proteins IL-6 (Fig 4G) and IL-8 (Fig 4H), a response that persisted for up to ten days, indicating a persistant response to the intial irradiation.

To further characterize the astrocytic response to radiation in culture, we performed RNA sequencing on primary astrocytes 24 h after receiving a dose of 0 Gy or 10 Gy radiation. Unsurprisingly, radiation had a profound effect on astrocyte gene expression. RNA sequencing analysis revealed distinct gene expression patterns that differ between control and irradiated astrocytes (Fig 4I), including an upregulation of the reactive astrocyte marker GFAP (p=4.6E-16). Analysis of gene set enrichment data revealed an atypical response to irradiation, including suppression of the p53 pathway (Supplementary Table 1), which has been previously reported.[43] Other notable changes to gene sets were those involved in DNA repair and cell cycle-related gene sets (Supplementary Table 1). This fits with previous reports that astrocytes respond to radiation by undergoing reactive gliosis, a state in which they often become proliferative. These findings

support the potential for astrocytes to survive irradiation and persist in the irradiated tumor volume where they might modify the microenvironment.

In addition to radiation response genes, a variety of gene sets involved in cancer were altered. Notably, gene sets associated with glioblastoma plasticity and gliomagenesis by PDGFB were upregulated, as were gene sets associated with the epithelial to mesenchymal transition, doxorubicin resistance, metastasis, and relapse in other cancer types (Supplementary Table 1). Interestingly, a gene signature consisting of the 100 most upregulated genes in irradiated astrocytes as compared to controls was significantly associated with worse survival in GBM, based on analysis of The Cancer Genome Atlas (TCGA) GBM dataset[44] (Fig 4J).

Irradiated astrocytes secrete TGM2 *in vitro* and *in vivo* after irradiation

To identify which proteins in the extracellular matrix might be responsible for the increased stemness and radioresistance of cells cultured on ADMi, we performed mass LC-MS/MS analysis on ADMc and ADMi (Fig 5A). Supplementary Table 2 lists proteins that changed significantly in matrix from irradiated astrocytes (summarized graphically in Figure 5A). While multiple proteins within the dataset provide promising leads in identifying a potential target within the ECM, we selected transglutaminase 2 (TGM2) for further inquiry. TGM2 is a multifunctional protein with transamidating, deamidation, and GTPase activity, as well as enzyme-independent scaffolding functions.[45] It cross-links fibronectin and has scaffolding functions with integrin β1, both of which are associated with radiation resistance and stemness,[46,47] and has recently been proposed to promote neurogensis from neural stem cells in the adult brain.[48] Its inhibition improved survival

11

in a glioma xenograft model[49] and it has been shown to be a prognostic indicator of shorter time to relapse after chemoradiotherapy.[50]

We first confirmed increased expression of TGM2 in matrix from multiple batches of astrocytes from different individuals by western blot (Fig 5B). We followed this by examining TGM2 expression *in vivo* in our genetic model of PDGFB-driven gliomagenesis (Fig 4A). Whole brain sections were stained for Olig2 (green), TGM2 (yellow), and GFAP (magenta) (Fig 5C-D). Relative to non-tumor bearing brain tissue, TGM2 expression was elevated in tumors (white bounded area, Fig 5C), was extensively expressed in the stromal compartment, and showed areas of co-staining with GFAP (Fig 5C, example: blue arrow, merged high magnification image). In the tumors treated with 10 Gy radiation (Fig 5D) TGM2 expression was retained in the likely original tumor volume and even increased, resulting in a greater percent area covered by TGM2 (Fig 5E) and increased ratio of TGM2 to Olig2 (Fig 5F) within the area of TGM2-positive staining compared to the non-irradiated brain. In the irradiated tumors, regions of TGM2 staining were also found in close association with GFAP-sitive astrocytes, often co-staining or showing astrocytes surrounding areas of intense TGM2-positivity (Fig 5D, example: blue arrow, merged high magnification image).

Another notable expression pattern for TGM2 demonstrates that, like GFAP, TGM2 expression is elevated in areas of microvascular proliferation and is closely associated with the vasculature (Fig 5G). Comparable to our findings in mice, analysis of the Ivy Glioblastoma Atlas Project (IVY-GAP), which examines gene expression within specific histologically defined regions of the

tumor,[51] reveals that TGM2 is highly elevated in areas of microvascular proliferation (Supplemental Figure 3).

Taken together, these data suggest that irradiation promotes increased expression of TGM2 from astrocytes, which may promote radiation resistance of glioma cells. Furthermore, because this high expression is retained even after the tumor bulk recedes, it potentially provides a radio-protective environment for a newly expanding tumor. We therefore returned to our *in vitro* experimental systems to determine if there was a functional relationship between TGM2 and stemness and radiation resistance of glioma cells.

Astrocyte-derived TGM2 promotes glioma stemness after irradiation

To determine whether TGM2 expression might be associated with glioma cell stemness or radiation resistance, we examined the effects of either purified TGM2 or TGM2 inhibitors on our *in vitro* model of glioma cell-astrocyte matrix interaction. We found that purified TGM2, when coated onto ADMc, could raise the SP of glioma cells near to that seen with glioma cells cultured on ADMi (Fig 6A). In contrast, inhibition of TGM2 with two different TGM2 inhibitors, GK921 (Fig 6B) and dansylcadaverine (DC; Fig 6C) decreased the SP of glioma cells cultured on ADMi to the levels seen on ADMc. GK921 also decreased survival after irradiation of glioma cells cultured on ADMi to levels seen on ADMc, while not affecting glioma cells cultured on ADMc (Fig 6D). These data suggest that TGM2 contributes to the increased stemness and radiation resistance of glioma cells cultured on ADMi as compared to those cultured on ADMc.

In vivo, tumors treated with 10 Gy radiation showed increased expression of CD44 (Fig 6 E-H), a stem cell marker in glioma[52] and a marker of mesenchymal subtype GBM, which strongly co-localized with TGM2 (Fig 6G-H). Like TGM2, CD44 expression was retained in the likely original tumor volume after irradiation, even as the Olig2-positive tumor cells receded, as seen by increased expression relative to Olig2 (Fig 6F). These data provide evidence that TGM2 expression is associated with increased stemness *in vivo*, which is elevated after irradiation.

TGM2 is a potential therapeutic target in GBM

To further examine the effects of TGM2 inhibition, we used an *ex vivo* organotypic slice model of GBM. We initiated tumors in our *Nestin-tv-a Ink4a/Arf⁺/⁻* mice by injection with RCAS-*PDGFB* and shp53, then sliced freshly-harvested brains from mice upon detection of brain tumor symptoms. These slices were cultured overnight, followed by treatment with either 0 μM or 5 μM of the TGM2 inhibitor GK921 for 72 h. Slices were fixed then cryosectioned, followed by immunofluorescent detection of Olig2 to determine the presence of tumor cells in the slices. Treatment of the slices with the TGM2 inhibitor significantly decreased the percent of Olig2-positive nuclei in the sections, in some cases reducing Olig2-positive cells to undetectable levels (Fig 7A-C).

In human glioma, TGM2 mRNA is elevated as tumor grade increases (Fig 7D). Likewise, TGM2 mRNA is significantly increased in isocitrate dehydrogenase wild type (IDHwt) tumors (Fig 7E), the most aggressive tumor classification under the 2016 WHO classification system of diffuse gliomas.[53] Elevated TGM2 correlates with shorter survival times in glioma (Fig 7F). Within

14

IDHwt GBM, tumors with the top 10% of TGM2 mRNA expression have the shortest survival times (Fig 7G). These data suggest that TGM2 may be a viable target in GBM.

Based on our findings, we suggest a model in which radiation stimulates tumor-associated astrocytes to secrete TGM2, which then promotes stemness and survival of glioma cells, allowing recurrence of the tumor (Fig 7F). Our findings suggest that inhibition of TGM2 signaling provides a potential new therapeutic target to sensitize glioma cells to radiotherapy and prevent recurrence (Fig 7F).

Discussion

GBM treatment options are extremely limited after tumor recurrence. As surgery can rarely eliminate all GBM cells, identifying and targeting pathways that support GBM cell survival after radiotherapy is essential to improving outcomes. Clinical findings indicate that a short course of radiotherapy over three weeks results in no clinically significant difference in outcomes when compared to a six-week course.[54,55] One interpretation of these data in light of findings presented here, is that neuroprotective pathways may be initiated in the brain in response to radiation, to protect cells from further radiation-induced damage, and that GBM cells can take advantage of this altered microenvironment. While many studies have begun examining how the tumor microenvironment can promote radiation resistance and associated GBM stemness,[28,56-59] little study has been made of how the stromal cells themselves respond to treatment modalities. This is an important question, as findings presented here suggest that stromal cells may respond to

15

radiation in ways which could prime the microenvironment for protection of glioma cells against further radiation insults.

This study provides a promising new strategy in GBM treatment by examining lasting changes to the tumor microenvironment made by stromal cells in response to radiotherapy, which might be supporting radiation resistance of GBM cells. In particular, we identify astrocytes as persisting within the original tumor volume after the tumor bulk is killed by radiation. Tumor-associated astrocytes react to the GBM microenvironment with an altered phenotype,[60] and were recently shown to promote glioma growth.[32,61] We show here that astrocytes secrete TGM2 in response to radiation, which supports stemness and radiation resistance of GBM cells. Inhibition of TGM2 decreased survival of tumor cells in an *ex vivo* organotypic slice model of GBM, and was previously shown to increase survival in a glioma xenograft model.[49] Our findings suggest a new strategy for sensitizing GBM cells to radiotherapy by short-circuiting the normal brain's protective response to radiation.

Materials and Methods

Generation of Murine Gliomas

Gliomas were induced in Nestin-*tv-a* or Nestin-*tv-a Ink4a/Arf*^{-/-} mice by injecting indicated combinations of RCAS-*PDGFB* and RCAS-shp53-transfected DF-1 cells (ATCC) intracranially in the brain as previously described.[62,63] Mice were monitored daily and euthanized upon exhibiting symptoms of glioma. The use of laboratory animals was conducted in accordance with European Union directive on the subject of animal rights. All animal experiments were approved

16

by the relevant local ethical committees (CEIyBA (CBA PA37_2013)/the Institutional Animal Care and Use Committee (IACUC 029-2013/001) (CNIO), M-186/14 (Lund), and 5.8.18-16350/2017 (Uppsala).

Cell Lines and Cultures

PIGPC were isolated as previously described.[17] PIGPC and U251 cells were cultured in DMEM (Corning Cat#10-014-CVR) supplemented with 10% FBS (Biological Industries Cat#04-007-1A) and 1% PenStrep (Corning Cat#30-002-CI). Primary Human Brain Vascular Pericytes (HBVP), (ScienCell, Cat. #1200) were cultured in PM (ScienCell, Cat. #1201) and were used below passage 4. Cells were grown as a monolayer on 2 µg/cm^2 poly-l-lysine mol wt 70,000-150,000 (PLL) (Sigma Cat. #P4707) coated plastic. Cells were subcultured using Trypsin/EDTA solution (Corning Cat. #25-053-CI) and Trypsin Neutralizing solution (ThermoFisher Cat. 1165862) followed by centrifugation 1000 RPM, 5 min, in 1 volume FBS (Biological Industries Cat#04-007-1A). Human brain microglia (HMC3) (ATCC Cat. # CRL-3304) were cultured in DMEM (Corning Cat#10-014-CVR) supplemented with 10% FBS (Biological Industries Cat#04-007-1A) and 1% PenStrep (Corning Cat#30-002-CI). Mouse brain endothelial cells (BEND3) (ATCC Cat. # CRL-2299) were cultured in Endothelial Cell Growth Medium MV2 (PromoCell Cat. #C-22121) and were grown as a monolayer on 0.1% gelatin coated plastic. Primary human astrocytes (3H Biomedical, Cat. #1800-10) were cultured in Human Astrocyte Medium (3H Biomedical, Cat. #SC1801) and were used below passage 15. U3082 primary glioma cells were obtained from HGCC (hgcc.se) and were cultured in DMEM/F12 with Glutamax supplemented with 1% PenStrep, N2, B27, EGF, and FGF (HGC Medium) as previously described [64]. Cells were grown

to subconfluence, dissociated with Accutase (StemPro, Cat #A11105) and grown either as neurospheres or monolayer on laminin-coated (BioLamina, Cat #LN521) plastic.

Immunofluorescence

Cryosections were fixed in 4% PFA followed by permeabilization in 0.3% Triton-x-100 and blocking in 1% BSA in PBS. Cryosections of organotypic slice cultures were fixed in 4% PFA followed by permeabilization in 0.1% Triton-x-100 and 0.1% sodium citrate. Sections were incubated overnight in 1% BSA in PBS with the following primary antibodies:

Figure	Antibodies
Fig. 1F-G	Rabbit anti-GFAP (DAKO, Z033401-2)
Fig. 2B-C	Rat anti-CD34 (eBiosciece, 14-0341-81)
Fig. 2E	Rabbit anti-Ki67 (ThermoFischer, 12683697)
Fig. 2G	Rat anti-CD34 (eBiosciece, 14-0341-81), rabbit anti-Olig2 (Merck, AB9610) and chicken anti-GFAP (AB4674, Abcam)
Fig. 4B	Rabbit anti-Olig2 (Merck, AB9610) and chicken anti-GFAP (AB4674, Abcam)
Fig. 4E	Rabbit anti-GFAP (DAKO, Z033401-2)
Fig. 4F	Rabbit anti-Vimentin (Abcam, AB45939)
Fig. 5C	Rabbit anti-Olig2 (Merck, AB9610), sheep anti-TGM2 (Novus Biologicals, AF5418), and rat anti-GFAP (Life Technologies, 130300)
Fig. 5G	Sheep anti-TGM2 (Novus Biologicals, AF5418) and Rat anti-CD34 (eBiosciece, 14-0341-81)
Fig. 6G-H	Rabbit anti-Olig2 (Merck, AB9610), sheep anti-TGM2 (Novus Biologicals, AF5418), and rat anti-GFAP (Life Technologies, 130300)
Fig. 7A-B	Goat anti-Olig2 (Novus, AF2418)

After washing, sections were incubated with the appropriate Alexafluor-conjugated secondary antibodies for 1 h: Donkey anti-sheep 647 (Abcam, AB150179), donkey anti-rat 568 (Abcam, AB175475), donkey anti-rat 488 (Invitrogen, 10123952), donkey anti-rabbit 488 (Invitrogen,

18

A21206), goat anti-chicken 568 (Invitrogen, 10462822). Images were acquired using an Olympus BX63 microscope and DP80 camera and cellSens Dimension v 1.12 software (Olympus Corporation).

Co-culture experiments

For co-culture experiments 100,000 (BEND3, HMC3 or PIGPC) or 50,000 (HBPV) cells were pretreated with or without 10 Gy radiation following 48h of co-culture with 100,000 PIGPC cells. Co-culture of microglia, pericytes, endothelial, or astrocytes cells and PIGPC cells was performed in DMEM.

Irradiation of cells

Irradiated pericytes, microglia, endothelial cells, and astrocytes were pretreated with 10 Gy irradiation in a CellRad x-ray cell irradiator (Faxitron).

Side Population Assay

For SP, cells were resuspended at 1×10^6 cells/ml and incubated at 37 °C, 30 minutes with or without 10 µM Fumitremorgin C (FTC) (Sigma). Cells were incubated for a further 90 minutes with 5 mg/ml Hoechst 33342 (Sigma) with periodic vortexing. Cells were analyzed on a FACSVerse instrument (BD) equipped with a 405 nm violet laser. Dual wavelength detection was performed using 448/45 (Hoechst 33342-blue) and 613/18 (Hoechst 33342-red) filters.

19

Generation of Astrocyte Derived Matrix

A confluent monolayer of astrocytes was irradiated with 0 Gy or 10 Gy followed by 10 days of culture on 0.2% gelatin in astrocyte medium supplemented with 50 µg/ml L-ascorbic acid (Sigma). After 10 days, plates were decellularized in 0.4 mM NH_4OH (Fluka), 0.5% Triton X-100 in PBS with 1 mM $CaCl_2$ and 0.5 mM $MgCl_2$ at 37 °C, washed with PBS containing 1 mM $CaCl_2$ and 0.5 mM $MgCl_2$, then treated with 10 µg/ml DNAse I (Roche) for 1 h at 37 °C. Plates were washed and stored in PBS containing 1 mM $CaCl_2$ and 0.5 mM $MgCl_2$ at 4 °C.

Western Blot

After preparation of astrocyte derived matrix on 6-well plates as described above, matrix was scraped into 175 µl 4X Laemmli buffer (Bio-Rad, 161-0747) containing 150 mM DTT and boiled for 10 min. Equal volumes of lysate were separated on 7.5% polyacrylamide gels followed by transfer to PVDF membranes and blocking with 5% non-fat dry milk in PBS. TGM2 immunodetection was performed using antibody to TGM2 (ab2386, Abcam) followed by detection with HRP-conjugated anti-mouse secondary antibody (ThermoFisher, 31430) and ECL substrate (ThermoFisher, 34095). Blots were visualized on the LAS-3000 Imager (Fujifilm) and quantified using ImageJ.

Sample preparation of Cell Derived Matrix

Cell derived matrix was solubilized for LC-MS/MS analysis according to Naba *et al.*[65] Briefly, ECM was washed three times with PBS followed by solubilization in 8 M urea and 10 mM DTT, with agitation for 2 h at 37 °C. Iodoacetamide was added to a final concentration of 25 mM followed by incubation in dark for 30 min at room temperature. Samples were deglycosylated by

20

diluting samples to 2 M urea with 100 mM ammonium bicarbonate (pH 8.0) followed by treatment with PNGaseF and incubation with agitation at 37 °C for 2 h. Samples were digested with Lys-C, 2 h at 37 °C with agitation, followed by trypsin digestion overnight with agitation at 37 °C and a second trypsin digestion the next morning, 2 h at 37 °C with agitation. Trypsin was inactivated by acidifying the sample with freshly prepared 50% trifluoro-acetic acid (TFA) to a pH < 2. Samples were centrifuged at 16,000 x g for 5 min at room temperature and supernatant was collected into low-binding tubes and stored at -20 °C. All reagents were mass spec grade.

Solid Phase Extraction with StageTips was performed according to the protocol of Rappsilber *et al*. [66] using home packed C18 reversed-phase columns. Eppendorf gel loader pipet Tip 20µl were packed with C18 membrane filter (millipore) and Applied Biosystems™ POROS™ Reversed-Phase Media (POROS™ 20 R1 Self-Pack™ Reversed Phase Resin). The Gel-loader tip was mounted with the C18 membrane filter using needle and then packed with about 10-15 µl of POROS 20 R1 suspension. After that the column was activated with 10µl 70% acetonitrile and 0.1% TFA and then equilibrated by two volumes of 10µl 2% acetonitrile and 0.1% TFA. The sample were loaded followed by a wash of 10 uL of 2% acetonitrile and 0.1% TFA, finally the peptides were eluted using 15 µl 70% acetonitrile and 0.1% TFA into low binding Eppendorf tubes. Samples were speedvac to dryness and kept at -20°C until analyzed on the LC-MS/MS system.

LC-MS/MS analysis

The samples were reconstituted by adding 20µl of 2% acetonitrile, 0.1% TFA and were run as triplicate injections on a Orbitrap Fusion Tribrid MS system (Thermo Scientific) equipped with a Proxeon Easy-nLC 1000 (Thermo Fisher). Injected peptides were trapped on an Acclaim PepMap

C18 column (3 µm particle size, 75 µm inner diameter x 20 mm length). After trapping, gradient elution of peptides was performed on an Acclaim PepMap C18 column (2 µm particle size, 75 µm inner diameter x 250 mm length). The outlet of the analytical column was coupled directly to the mass spectrometer using a Proxeon nanospray source. The mobile phases for LC separation were 0.1% (v/v) formic acid in LC-MS grade water (solvent A) and 0.1% (v/v) formic acid in acetonitrile (solvent B). Peptides were first loaded with a constant pressure mode of solvent A onto the trapping column. Subsequently, peptides were eluted via the analytical column at a constant flow of 300 nL/min. During the elution step, the percentage of solvent B increased from 5% to 10% in the first 2 minutes, then increased to 25% in 50 minutes and then increased to 60% in 15 minutes and then increased to 90% in 5 minutes finally to 90% in a further 5 minutes. The peptides were introduced into the Orbitrap via a Stainless steel emitter 40 mm (Thermo Fisher) and a spray voltage of 2 kV was applied. The capillary temperature was set at 275 °C.

Data acquisition was carried out using a top N based data-dependent method with a cycle time of 3 seconds. The master scan was performed in the Orbitrap in the range of 350–1350 *m/z* at a resolution of 120,000 FWHM. The filling time was set at maximum of 50 ms with limitation of 4 x 10^5 ions. Ion trap CID-MS2 was acquired using normal mode, filling time maximum 60 ms with limitation of 7 x 10^3 ions, a precursor ion isolation width of 0.7 *m/z* and a rapid Ion trap scan was selected. Normalized collision energy was set to 27%. Only multiply charged (2^+ to 5^+) precursor ions were selected for MS2. The dynamic exclusion list was set to 30 s and relative mass window of 5ppm.

Data analysis

MS/MS spectra were searched with PEAKS (8.5) using UniProt Human database. Trypsin was used and 2 missed cleavages were allowed. 15 ppm precursor and 0.5 Da fragment tolerance were used as mass tolerance. Oxidation (M) and deamidation (NQ) were treated as dynamic modification and carbamidomethylation (C) as a fixed modification. Maximum number of PTM per peptide was set to three. Matrix proteins with at least 2 unique peptides and a protein significance score > 50 were included in the results.

Colony Assay

U251 cells were plated at 200 cells per well in a 6-well dish or 35 mm plate on ADMc or ADMi in DMEM. After 24 h, plates were irradiated with either 0 Gy or 4 Gy. Cells were cultured for 2 weeks or until visible colonies formed. Colonies were fixed in 4% PFA then stained with 0.01% Crystal Violet for 1 hr. Colonies were photographed on a LAS-3000 imaging system, then counted using Image J followed by visual confirmation (to reduce interference from background staining of matrix proteins).

Self-Renewal Assay

U3082 cells were cultured on ADMc or ADMi for 5 days in HGC Media. For primary spheres, cells were dissociated with Accutase then replated in 3 wells each of 6-well dishes at 300 cells/ml in 2 ml HGC Media and cultured until visible spheres formed, typically between 14 and 18 days. Primary spheres were visualized and counted on a Zeiss AX10 inverted microscope, then dissociated with Accutase and re-plated as described above. Secondary spheres were photographed on a Zeiss AX10 inverted microscope and counted.

23

RNA Sequencing Analyses

Sequencing performed at the Center for Translational Genomics, Lund University and Clinical Genomics Lund, SciLifeLab, and National Genomics Infrastructure Stockholm Node, Science for Life Laboratory. Raw count data was imported and analyzed using R statistic language (version 3.3.2). Data was rlog-normalized and combat corrected for experimental batch using DESeq2 and sva packages, respectively. DESeq differential expression analysis was performed on non-normalized raw counts. Genes with Benjamini adjusted p-values of <0.05 were considered differentially expressed. All genes ranked according to DESeq statistic (positive associated with highly expressed in irradiated astrocytes) and gene set enrichment analysis (GSEA)[67] was applied using the c2.all.v6.0 curated gene sets (MsidDB; broad.mit.edu/gsea/msigdb).

Patient cohort analysis

The R2: Genomics Analysis and Visualization Platform (http://r2.amc.nl) was used to examine the Glioblasoma-TCGA-540 dataset.[44] Astrocyte irradiation signature score was calculated using the z-score of the top 100 upregulated genes. Kaplan-Meier analysis using the scanning method was applied to the signature score using overall survival data and Bonferoni adjusted p-values of <0.05 was considered significant. Data from the Allen Institute for Brain Science IVY-GAP (available at http://glioblastoma.alleninstitute.org) were analyzed using the GlioVis data portal for visualization and analysis of brain tumor expression datasets.[51,68]

Culture in Sodium Alginate

Human astrocytes or PIGPCs were dissociated and counted. The cells were centrifuged at 0.5 x g for 5 minutes and resuspended in sodium alginate (Aldrich chemistry) 4:5 with cell culture medium. The cells were then added dropwise in medium containing 0.1 M $CaCl_2$, which leads to the formation of hydrogel beads. The beads were allowed to settle for ten minutes at 37° C, 5% CO_2 and then the medium was changed to new AM or DMEM.

Organotypic Slice Culture

Tumor-bearing brains from *Nestin-tv-a Ink4a/Arf$^{-/-}$* mice injected with RCAS-*PDGFB* and shp53 were sacrificed upon detection of brain tumor symptoms. Freshly dissected brains were sliced into 300 μm slices using a 5100 mz vibrating blade tissue slicer (Campden Instruments Ltd.). Slices were supported on polycarbonate tissue culture dish inserts with 0.4 μm pore size for culture at 37^oC, 5% CO_2 in DMEM/F12 with Glutamax supplemented with 1% PenStrep, N2, B27, EGF, and FGF (HGC Medium). After overnight incubation, slices were treated with either 0 μM or 5 μM of the TGM2 inhibitor GK921 daily for 72 h. Slices were fixed then cryosectioned, followed by immunofluorescent detection of Olig2 to determine the presence of tumor cells in the slices. Percent Olig2-positive nuclei were quantified using Cell Profiler.[69]

Acknowledgements

References

1   Stupp, R. *et al.* Effects of radiotherapy with concomitant and adjuvant temozolomide versus radiotherapy alone on survival in glioblastoma in a randomised phase III study: 5-year analysis of the EORTC-NCIC trial. *Lancet Oncol* **10**, 459-466, doi:10.1016/S1470-2045(09)70025-7 (2009).

2   Huse, J. T. & Holland, E. C. Targeting brain cancer: advances in the molecular pathology of malignant glioma and medulloblastoma. *Nature reviews. Cancer* **10**, 319-331, doi:10.1038/nrc2818 (2010).

3   Hess, C. F., Schaaf, J. C., Kortmann, R. D., Schabet, M. & Bamberg, M. Malignant glioma: patterns of failure following individually tailored limited volume irradiation. *Radiotherapy and oncology : journal of the European Society for Therapeutic Radiology and Oncology* **30**, 146-149 (1994).

4   Lathia, J. D., Mack, S. C., Mulkearns-Hubert, E. E., Valentim, C. L. & Rich, J. N. Cancer stem cells in glioblastoma. *Genes & development* **29**, 1203-1217, doi:10.1101/gad.261982.115 (2015).

5   Bao, S. *et al.* Glioma stem cells promote radioresistance by preferential activation of the DNA damage response. *Nature* **444**, 756-760, doi:10.1038/nature05236 (2006).

6   Verhaak, R. G. *et al.* Integrated genomic analysis identifies clinically relevant subtypes of glioblastoma characterized by abnormalities in PDGFRA, IDH1, EGFR, and NF1. *Cancer cell* **17**, 98-110, doi:10.1016/j.ccr.2009.12.020 (2010).

7   Neftel, C. *et al.* An Integrative Model of Cellular States, Plasticity, and Genetics for Glioblastoma. *Cell* **178**, 835-849.e821, doi:10.1016/j.cell.2019.06.024 (2019).

8   Liau, B. B. *et al.* Adaptive Chromatin Remodeling Drives Glioblastoma Stem Cell Plasticity and Drug Tolerance. *Cell stem cell* **20**, 233-246.e237, doi:10.1016/j.stem.2016.11.003 (2017).

9   Dirkse, A. *et al.* Stem cell-associated heterogeneity in Glioblastoma results from intrinsic tumor plasticity shaped by the microenvironment. *Nat Commun* **10**, 1787, doi:10.1038/s41467-019-09853-z (2019).

10   Minata, M. *et al.* Phenotypic Plasticity of Invasive Edge Glioma Stem-like Cells in Response to Ionizing Radiation. *Cell reports* **26**, 1893-1905.e1897, doi:10.1016/j.celrep.2019.01.076 (2019).

11   Segerman, A. *et al.* Clonal Variation in Drug and Radiation Response among Glioma-Initiating Cells Is Linked to Proneural-Mesenchymal Transition. *Cell reports* **17**, 2994-3009, doi:10.1016/j.celrep.2016.11.056 (2016).

12   Balca-Silva, J. *et al.* The Expression of Connexins and SOX2 Reflects the Plasticity of Glioma Stem-Like Cells. *Transl Oncol* **10**, 555-569, doi:10.1016/j.tranon.2017.04.005 (2017).

13   Pistollato, F. *et al.* Intratumoral hypoxic gradient drives stem cells distribution and MGMT expression in glioblastoma. *Stem Cells* **28**, 851-862, doi:10.1002/stem.415 (2010).

14   Easwaran, H., Tsai, H. C. & Baylin, S. B. Cancer epigenetics: tumor heterogeneity, plasticity of stem-like states, and drug resistance. *Mol Cell* **54**, 716-727, doi:10.1016/j.molcel.2014.05.015 (2014).

15   Safa, A. R., Saadatzadeh, M. R., Cohen-Gadol, A. A., Pollok, K. E. & Bijangi-Vishehsaraei, K. Glioblastoma stem cells (GSCs) epigenetic plasticity and interconversion between differentiated non-GSCs and GSCs. *Genes Dis* **2**, 152-163, doi:10.1016/j.gendis.2015.02.001 (2015).

16   Li, Z. *et al.* Hypoxia-inducible factors regulate tumorigenic capacity of glioma stem cells. *Cancer cell* **15**, 501-513, doi:10.1016/j.ccr.2009.03.018 (2009).

17   Pietras, A. *et al.* Osteopontin-CD44 signaling in the glioma perivascular niche enhances cancer stem cell phenotypes and promotes aggressive tumor growth. *Cell stem cell* **14**, 357-369, doi:10.1016/j.stem.2014.01.005 (2014).

18   Motegi, H., Kamoshima, Y., Terasaka, S., Kobayashi, H. & Houkin, K. Type 1 collagen as a potential niche component for CD133-positive glioblastoma cells. *Neuropathology : official journal of the Japanese Society of Neuropathology* **34**, 378-385, doi:10.1111/neup.12117 (2014).

19   Yu, Q. *et al.* Fibronectin Promotes the Malignancy of Glioma Stem-Like Cells Via Modulation of Cell Adhesion, Differentiation, Proliferation and Chemoresistance. *Front Mol Neurosci* **11**, 130, doi:10.3389/fnmol.2018.00130 (2018).

20   Farace, C. *et al.* Microenvironmental Modulation of Decorin and Lumican in Temozolomide-Resistant Glioblastoma and Neuroblastoma Cancer Stem-Like Cells. *PloS one* **10**, e0134111, doi:10.1371/journal.pone.0134111 (2015).

21   Jiang, X., Zhou, T., Wang, Z., Qi, B. & Xia, H. HSP47 Promotes Glioblastoma Stemlike Cell Survival by Modulating Tumor Microenvironment Extracellular Matrix through TGF-beta Pathway. *ACS Chem Neurosci* **8**, 128-134, doi:10.1021/acschemneuro.6b00253 (2017).

22   Lathia, J. D. *et al.* Laminin alpha 2 enables glioblastoma stem cell growth. *Ann Neurol* **72**, 766-778, doi:10.1002/ana.23674 (2012).

23   Li, Y. *et al.* SERPINA3 induced by astroglia/microglia co-culture facilitates glioblastoma stem-like cell invasion. *Oncol Lett* **15**, 285-291, doi:10.3892/ol.2017.7275 (2018).

24   Pointer, K. B. *et al.* Association of collagen architecture with glioblastoma patient survival. *J Neurosurg* **126**, 1812-1821, doi:10.3171/2016.6.Jns152797 (2017).

25   Barnes, J. M. *et al.* A tension-mediated glycocalyx-integrin feedback loop promotes mesenchymal-like glioblastoma. *Nat Cell Biol* **20**, 1203-1214, doi:10.1038/s41556-018-0183-3 (2018).

26   Charles, N. *et al.* Perivascular nitric oxide activates notch signaling and promotes stem-like character in PDGF-induced glioma cells. *Cell stem cell* **6**, 141-152, doi:10.1016/j.stem.2010.01.001 (2010).

27   Wang, X. *et al.* Reciprocal Signaling between Glioblastoma Stem Cells and Differentiated Tumor Cells Promotes Malignant Progression. *Cell stem cell* **22**, 514-528.e515, doi:10.1016/j.stem.2018.03.011 (2018).

28   Hide, T., Shibahara, I. & Kumabe, T. Novel concept of the border niche: glioblastoma cells use oligodendrocytes progenitor cells (GAOs) and microglia to acquire stem cell-like features. *Brain Tumor Pathol* **36**, 63-73, doi:10.1007/s10014-019-00341-2 (2019).

29   Calabrese, C. *et al.* A perivascular niche for brain tumor stem cells. *Cancer cell* **11**, 69-82, doi:10.1016/j.ccr.2006.11.020 (2007).

30   Hambardzumyan, D. & Bergers, G. Glioblastoma: Defining Tumor Niches. *Trends in cancer* **1**, 252-265, doi:10.1016/j.trecan.2015.10.009 (2015).

31   Quail, D. F. & Joyce, J. A. The Microenvironmental Landscape of Brain Tumors. *Cancer cell* **31**, 326-341, doi:10.1016/j.ccell.2017.02.009 (2017).

32   Mega, A. *et al.* Astrocytes enhance glioblastoma growth. *Glia* **68**, 316-327, doi:10.1002/glia.23718 (2020).

33   Pyonteck, S. M. *et al.* CSF-1R inhibition alters macrophage polarization and blocks glioma progression. *Nat Med* **19**, 1264-1272, doi:10.1038/nm.3337 (2013).

34   Patrawala, L. *et al.* Side population is enriched in tumorigenic, stem-like cancer cells, whereas ABCG2+ and ABCG2- cancer cells are similarly tumorigenic. *Cancer research* **65**, 6207-6219, doi:10.1158/0008-5472.Can-05-0592 (2005).

35   Ho, M. M., Ng, A. V., Lam, S. & Hung, J. Y. Side population in human lung cancer cell lines and tumors is enriched with stem-like cancer cells. *Cancer research* **67**, 4827-4833, doi:10.1158/0008-5472.Can-06-3557 (2007).

36   Goodell, M. A., Brose, K., Paradis, G., Conner, A. S. & Mulligan, R. C. Isolation and functional properties of murine hematopoietic stem cells that are replicating in vivo. *The Journal of experimental medicine* **183**, 1797-1806 (1996).

37   Bleau, A. M. *et al.* PTEN/PI3K/Akt pathway regulates the side population phenotype and ABCG2 activity in glioma tumor stem-like cells. *Cell stem cell* **4**, 226-235, doi:10.1016/j.stem.2009.01.007 (2009).

38   Chiang, C. S., McBride, W. H. & Withers, H. R. Radiation-induced astrocytic and microglial responses in mouse brain. *Radiotherapy and oncology : journal of the European Society for Therapeutic Radiology and Oncology* **29**, 60-68 (1993).

39   Noel, F. & Tofilon, P. J. Astrocytes protect against X-ray-induced neuronal toxicity in vitro. *Neuroreport* **9**, 1133-1137 (1998).

40   Schneider, L., Fumagalli, M. & d'Adda di Fagagna, F. Terminally differentiated astrocytes lack DNA damage response signaling and are radioresistant but retain DNA

repair proficiency. *Cell death and differentiation* **19**, 582-591, doi:10.1038/cdd.2011.129 (2012).

41   Sofroniew, M. V. & Vinters, H. V. Astrocytes: biology and pathology. *Acta neuropathologica* **119**, 7-35, doi:10.1007/s00401-009-0619-8 (2010).

42   Liddelow, S. A. & Barres, B. A. Reactive Astrocytes: Production, Function, and Therapeutic Potential. *Immunity* **46**, 957-967, doi:10.1016/j.immuni.2017.06.006 (2017).

43   Gong, L. *et al.* Differential radiation response between normal astrocytes and glioma cells revealed by comparative transcriptome analysis. *OncoTargets and therapy* **10**, 5755-5764, doi:10.2147/ott.S144002 (2017).

44   Comprehensive genomic characterization defines human glioblastoma genes and core pathways. *Nature* **455**, 1061-1068, doi:10.1038/nature07385 (2008).

45   Tabolacci, C., De Martino, A., Mischiati, C., Feriotto, G. & Beninati, S. The Role of Tissue Transglutaminase in Cancer Cell Initiation, Survival and Progression. *Medical sciences (Basel, Switzerland)* **7**, doi:10.3390/medsci7020019 (2019).

46   Condello, S. *et al.* Tissue Tranglutaminase Regulates Interactions between Ovarian Cancer Stem Cells and the Tumor Niche. *Cancer research* **78**, 2990-3001, doi:10.1158/0008-5472.Can-17-2319 (2018).

47   Bagatur, Y., Ilter Akulke, A. Z., Bihorac, A., Erdem, M. & Telci, D. Tissue transglutaminase expression is necessary for adhesion, metastatic potential and cancer stemness of renal cell carcinoma. *Cell adhesion & migration* **12**, 138-151, doi:10.1080/19336918.2017.1322255 (2018).

48   Kjell, J. *et al.* Defining the Adult Neural Stem Cell Niche Proteome Identifies Key Regulators of Adult Neurogenesis. *Cell stem cell* **26**, 277-293.e278 (2020).

49   Yin, J. *et al.* Transglutaminase 2 Inhibition Reverses Mesenchymal Transdifferentiation of Glioma Stem Cells by Regulating C/EBPbeta Signaling. *Cancer research* **77**, 4973-4984, doi:10.1158/0008-5472.Can-17-0388 (2017).

50   Deininger, M. H., Grote, E., Wickboldt, J. & Meyermann, R. Distinct radiochemotherapy protocols differentially influence cellular proliferation and expression of p53 and Bcl-2 in glioblastoma multiforme relapses in vivo. *Journal of neuro-oncology* **48**, 121-129 (2000).

51   Puchalski, R. B. *et al.* An anatomic transcriptional atlas of human glioblastoma. *Science* **360**, 660-663, doi:10.1126/science.aaf2666 (2018).

52   Anido, J. *et al.* TGF-beta Receptor Inhibitors Target the CD44(high)/Id1(high) Glioma-Initiating Cell Population in Human Glioblastoma. *Cancer cell* **18**, 655-668, doi:10.1016/j.ccr.2010.10.023 (2010).

53   Louis, D. N. *et al.* The 2016 World Health Organization Classification of Tumors of the Central Nervous System: a summary. *Acta neuropathologica* **131**, 803-820, doi:10.1007/s00401-016-1545-1 (2016).

54   Roa, W. *et al.* Abbreviated course of radiation therapy in older patients with glioblastoma multiforme: a prospective randomized clinical trial. *Journal of clinical oncology : official journal of the American Society of Clinical Oncology* **22**, 1583-1588, doi:10.1200/jco.2004.06.082 (2004).

55   Roa, W. *et al.* International Atomic Energy Agency Randomized Phase III Study of Radiation Therapy in Elderly and/or Frail Patients With Newly Diagnosed Glioblastoma Multiforme. *Journal of clinical oncology : official journal of the American Society of Clinical Oncology* **33**, 4145-4150, doi:10.1200/jco.2015.62.6606 (2015).

56   Li, D. *et al.* Glioma-associated human endothelial cell-derived extracellular vesicles specifically promote the tumourigenicity of glioma stem cells via CD9. *Oncogene* **38**, 6898-6912, doi:10.1038/s41388-019-0903-6 (2019).

57   Silver, D. J. & Lathia, J. D. Therapeutic Injury and Tumor Regrowth: Tumor Resection and Radiation Establish the Recurrent Glioblastoma Microenvironment. *EBioMedicine* **31**, 13-14, doi:10.1016/j.ebiom.2018.04.016 (2018).

58   Bhat, K. P. L. *et al.* Mesenchymal differentiation mediated by NF-kappaB promotes radiation resistance in glioblastoma. *Cancer cell* **24**, 331-346, doi:10.1016/j.ccr.2013.08.001 (2013).

59   Jamal, M., Rath, B. H., Williams, E. S., Camphausen, K. & Tofilon, P. J. Microenvironmental regulation of glioblastoma radioresponse. *Clin Cancer Res* **16**, 6049-6059, doi:10.1158/1078-0432.Ccr-10-2435 (2010).

60   Katz, A. M. *et al.* Astrocyte-specific expression patterns associated with the PDGF-induced glioma microenvironment. *PloS one* **7**, e32453, doi:10.1371/journal.pone.0032453 (2012).

61   Priego, N. *et al.* STAT3 labels a subpopulation of reactive astrocytes required for brain metastasis. *Nat Med* **24**, 1024-1035, doi:10.1038/s41591-018-0044-4 (2018).

62   Holland, E. C., Hively, W. P., DePinho, R. A. & Varmus, H. E. A constitutively active epidermal growth factor receptor cooperates with disruption of G1 cell-cycle arrest pathways to induce glioma-like lesions in mice. *Genes & development* **12**, 3675-3685, doi:10.1101/gad.12.23.3675 (1998).

63   Ozawa, T. *et al.* Most human non-GCIMP glioblastoma subtypes evolve from a common proneural-like precursor glioma. *Cancer cell* **26**, 288-300, doi:10.1016/j.ccr.2014.06.005 (2014).

64   Xie, Y. *et al.* The Human Glioblastoma Cell Culture Resource: Validated Cell Models Representing All Molecular Subtypes. *EBioMedicine* **2**, 1351-1363, doi:10.1016/j.ebiom.2015.08.026 (2015).

65   Naba, A., Clauser, K. R. & Hynes, R. O. Enrichment of Extracellular Matrix Proteins from Tissues and Digestion into Peptides for Mass Spectrometry Analysis. *Journal of visualized experiments : JoVE*, e53057, doi:10.3791/53057 (2015).

66   Rappsilber, J., Mann, M. & Ishihama, Y. Protocol for micro-purification, enrichment, pre-fractionation and storage of peptides for proteomics using StageTips. *Nature protocols* **2**, 1896-1906, doi:10.1038/nprot.2007.261 (2007).

67   Subramanian, A. *et al.* Gene set enrichment analysis: a knowledge-based approach for interpreting genome-wide expression profiles. *Proceedings of the National Academy of Sciences of the United States of America* **102**, 15545-15550, doi:10.1073/pnas.0506580102 (2005).

68   Bowman, R. L., Wang, Q., Carro, A., Verhaak, R. G. & Squatrito, M. GlioVis data portal for visualization and analysis of brain tumor expression datasets. *Neuro-oncology* **19**, 139-141, doi:10.1093/neuonc/now247 (2017).

69   Carpenter, A. E. *et al.* CellProfiler: image analysis software for identifying and quantifying cell phenotypes. *Genome Biol* **7**, R100, doi:10.1186/gb-2006-7-10-r100 (2006).
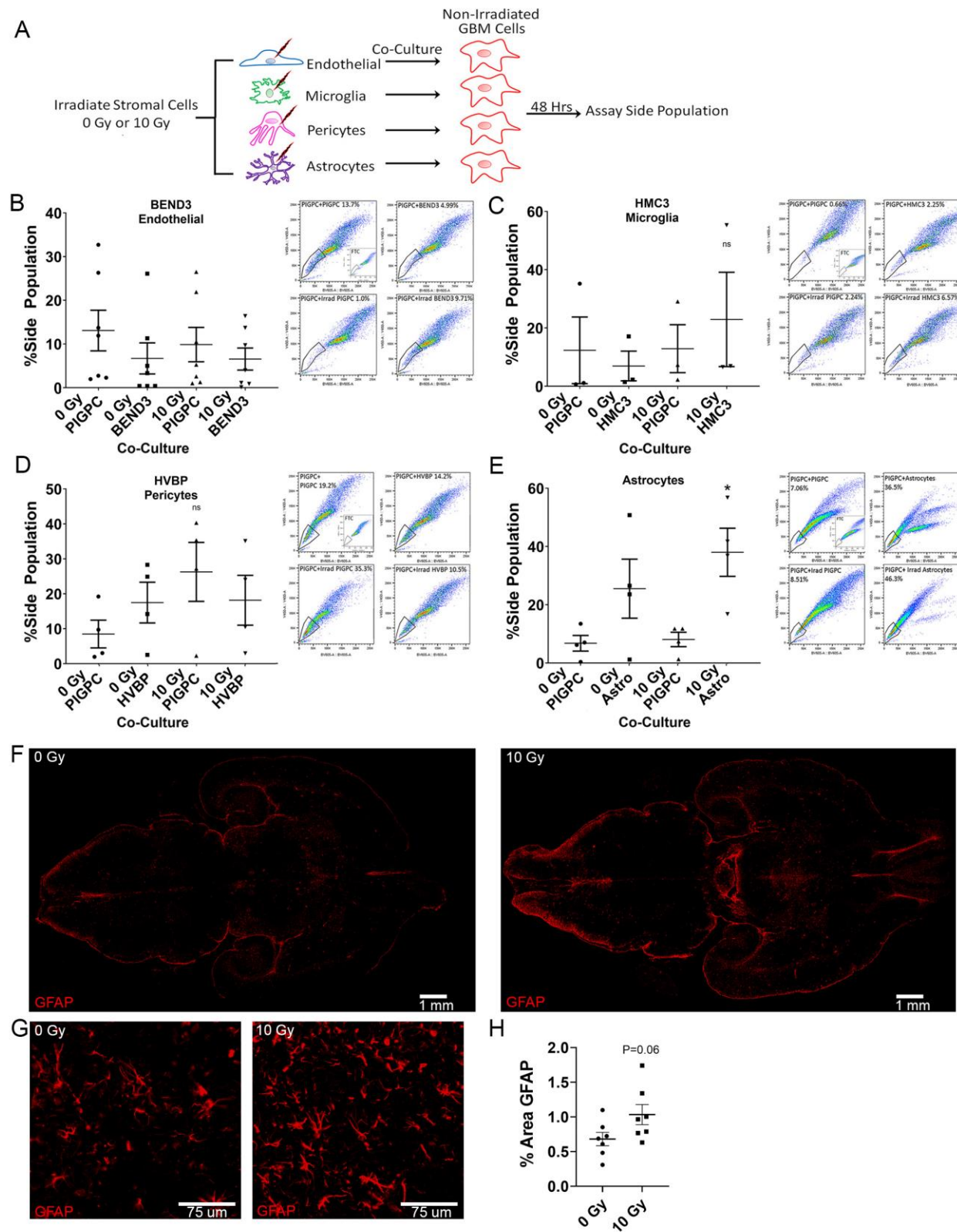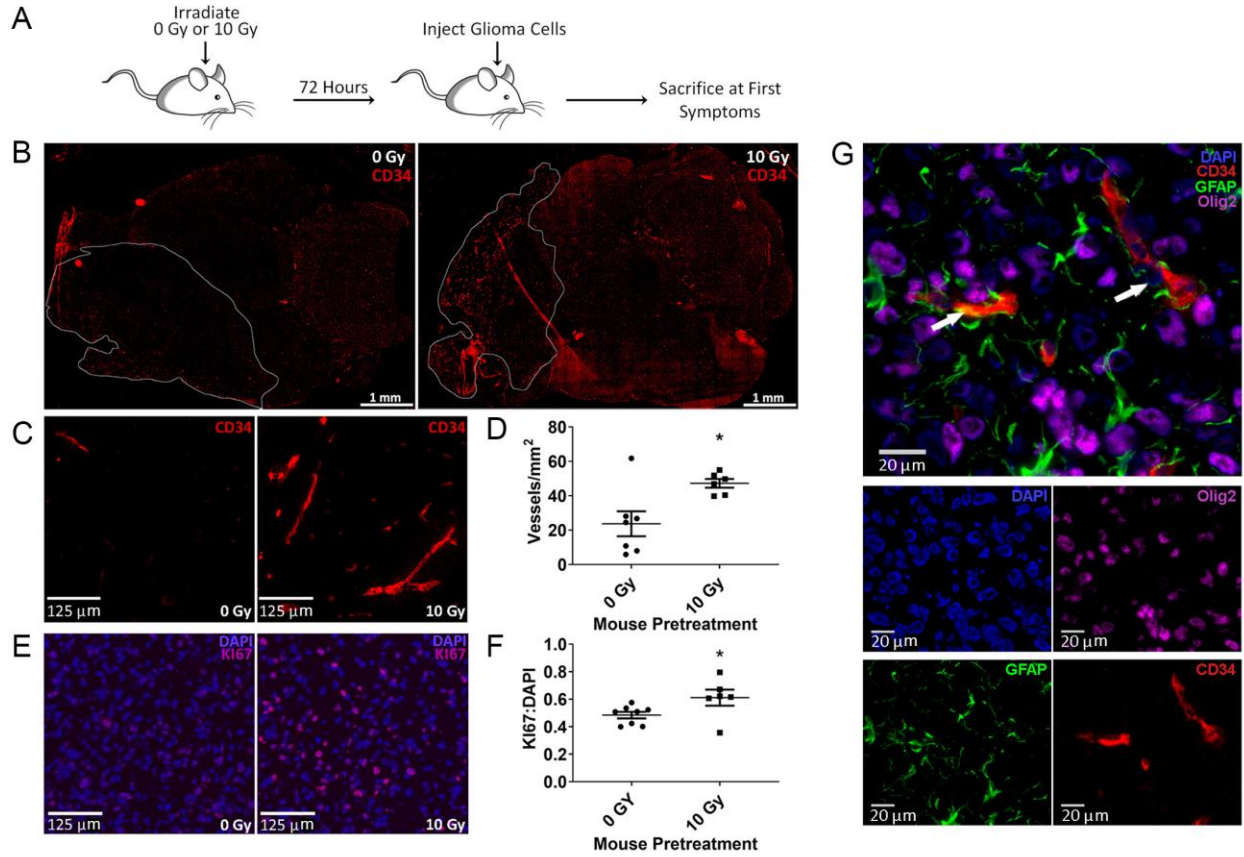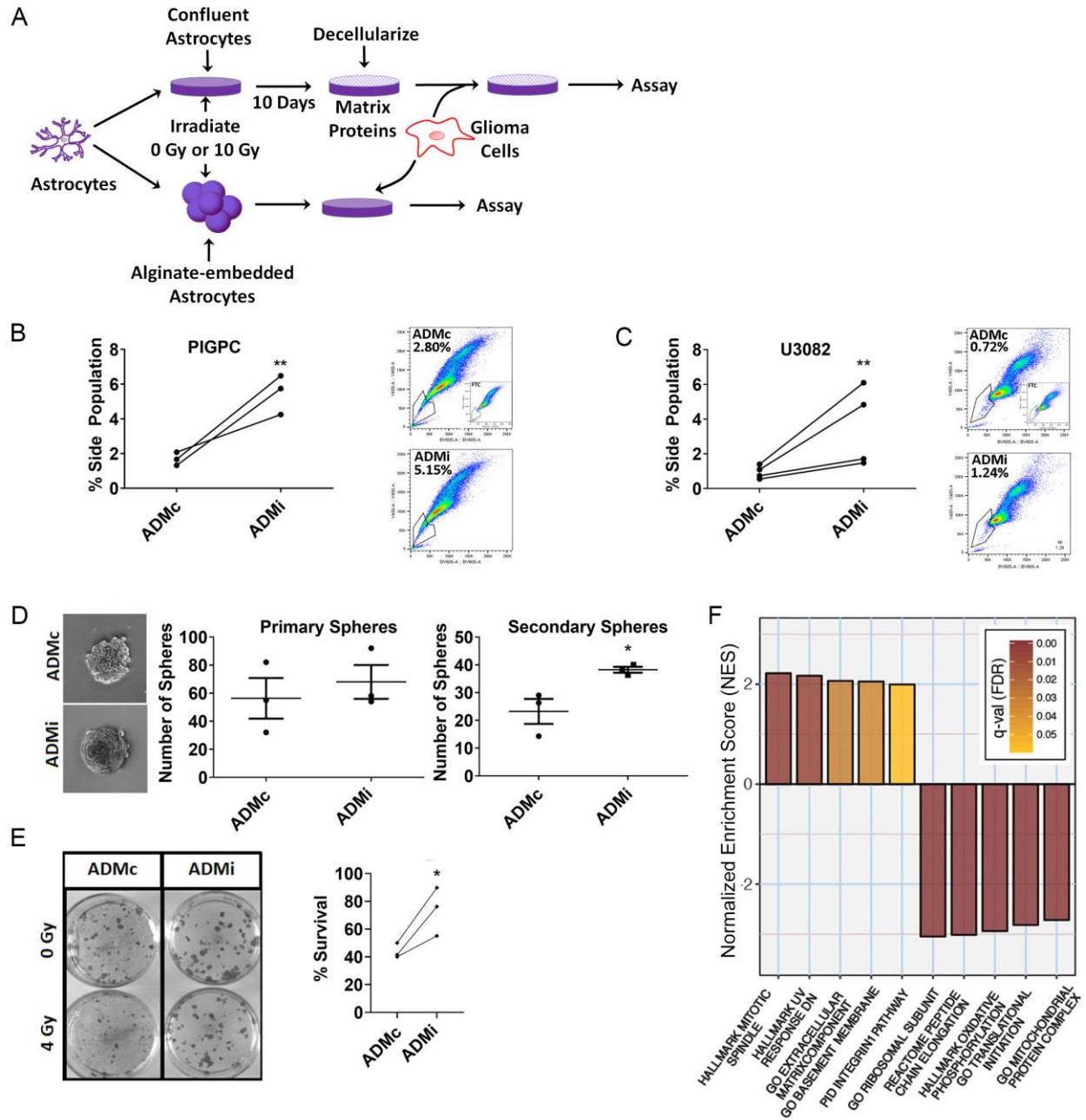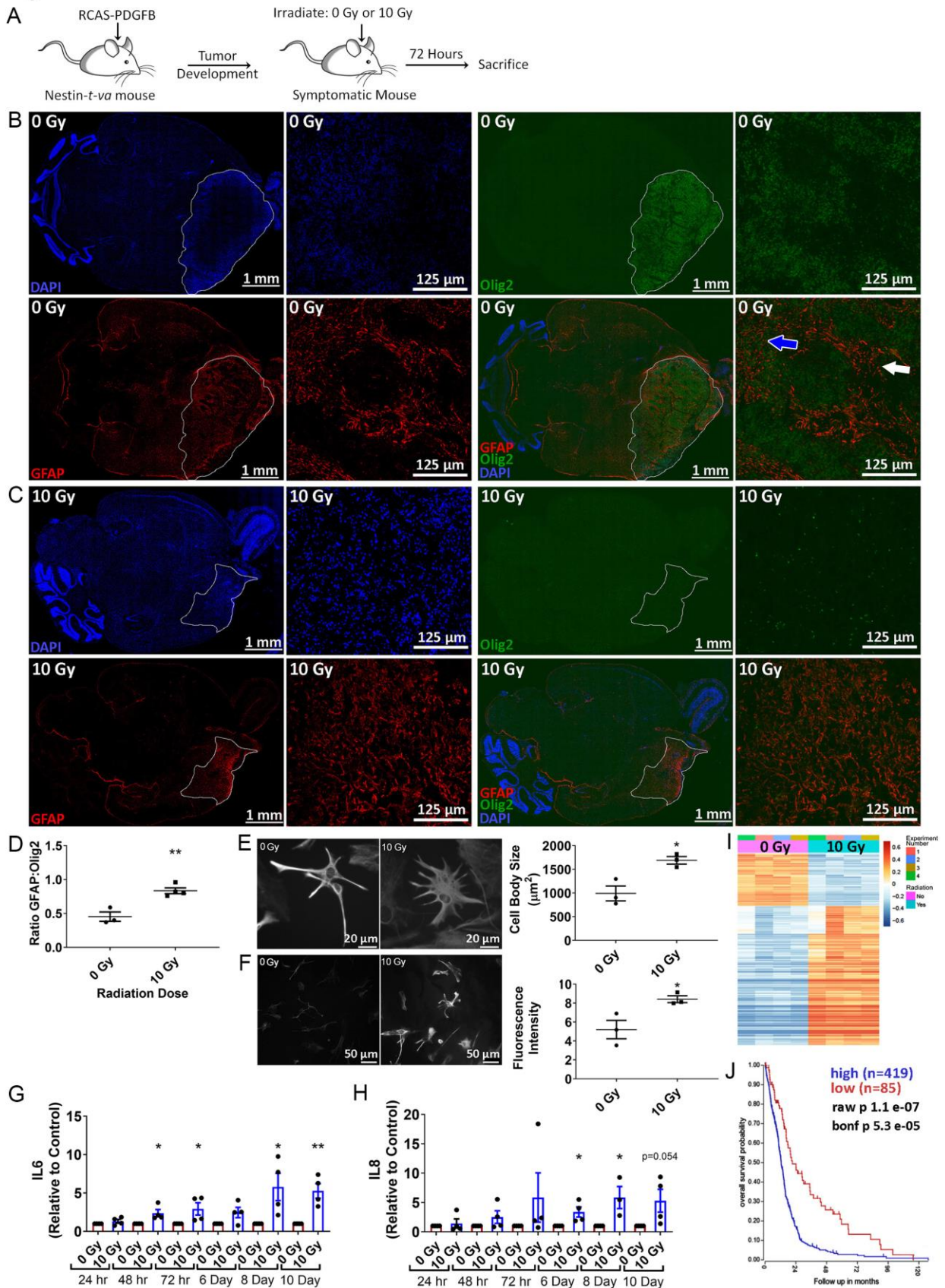
Figure 1

Figure 2
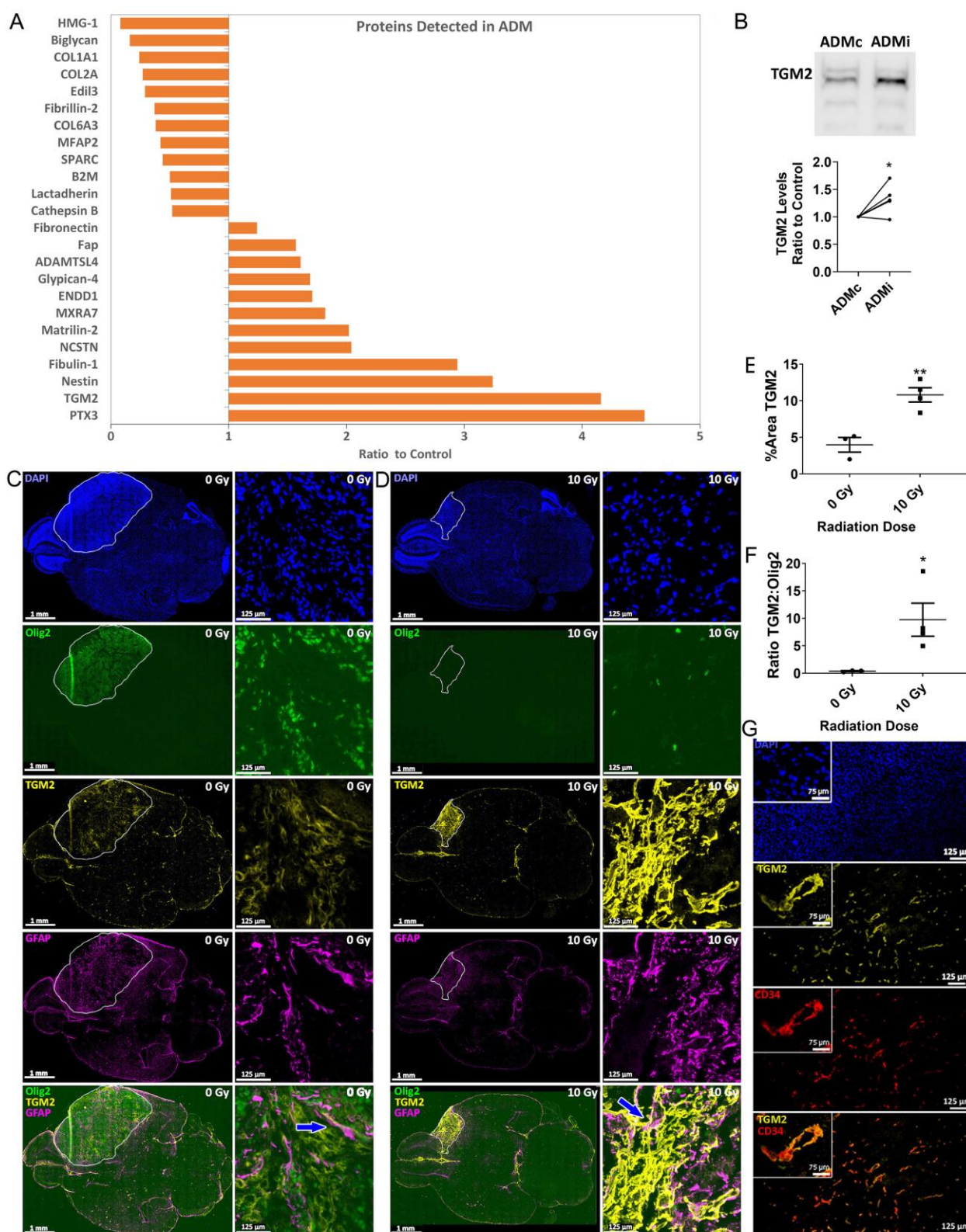
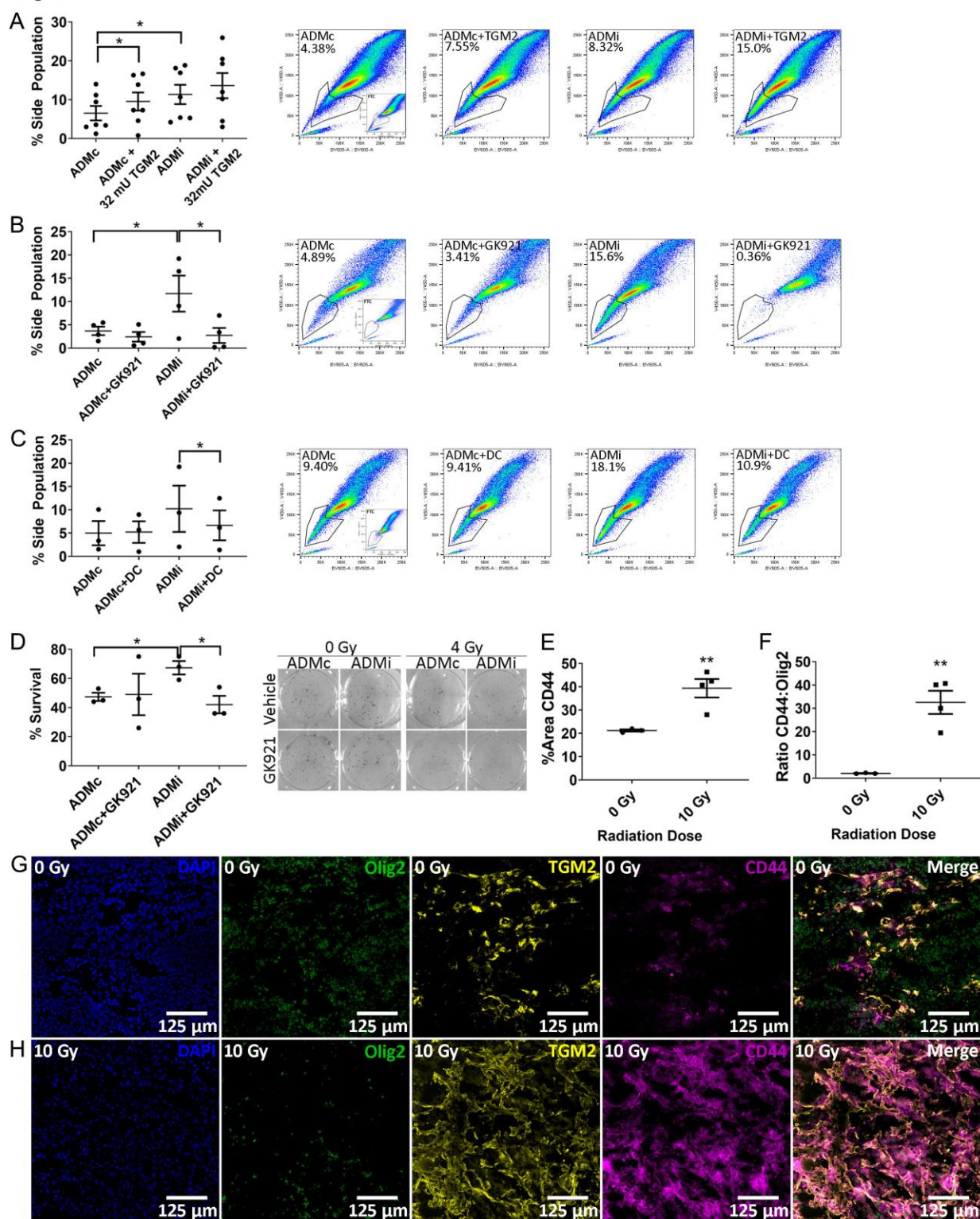## Figure 3

Figure 4
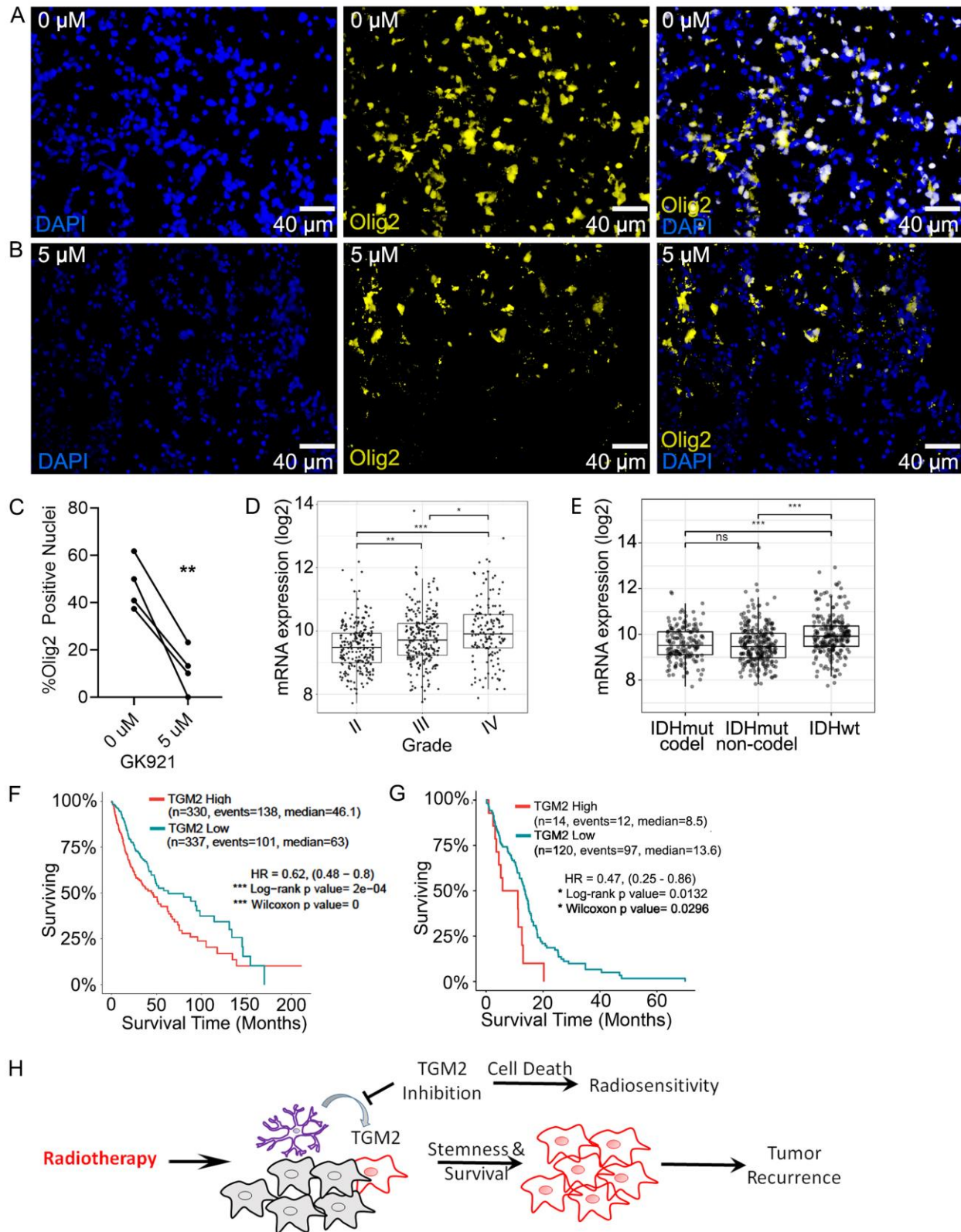

34

Figure 5

Figure 6

Figure 7

Figure Legends

Figure 1. Irradiated astrocytes promote glioma cell stemness

A) Experimental design. B-E) SP of PIGPC after co-culture with the indicated cell type pre-treated with the indicated radiation dose. Dots represent individual experiments and bars represents average of all experiments with SEM. Sample FACS plots show gating for SP. B) SP of PIGPC after co-culture with either 0 Gy-treated PIGPC (0 Gy PIGPC), 0 Gy-treated BEND3 endothelial cells (0 Gy BEND3), 10 Gy-treated PIGPC cells (10 Gy PIGPC), or 10 Gy-treated BEND3 endothelial cells (10 Gy BEND3). C) SP of PIGPC after co-culture with either 0 Gy PIGPC, 0 Gy-treated HMC3 microglia (0 Gy HMC3), 10 Gy PIGPC, or 10 Gy-treated HMC3 cells (10 Gy HMC3). D) SP of PIGPC after co-culture with either 0 Gy PIGPC, 0 Gy-treated HVBP pericytes (0 Gy HVBP), 10 Gy PIGPC, or 10 Gy-treated HVBP cells (10 Gy HVBP). E) SP of PIGPC after co-culture with either 0 Gy PIGPC, 0 Gy-treated astrocytes (0 Gy Astro), 10 Gy PIGPC, or 10 Gy-treated Astrocytes (10 Gy Astro). * $P \leq 0.05$ by one-way ANOVA with Dunnet's multiple comparison's post-test. F) Representative immunofluorescent detection of GFAP on whole brain scans of sections from non-tumor bearing mice treated with either 0 Gy or 10 Gy radiation. G) High magnification image of GFAP-positive cells from F. H) Percent area GFAP staining in 0 Gy and 10 Gy treated mice. Dots represent individual mice and bar represents average of all mice with SEM. P value represents results of Student's t-test.

Figure 2. The irradiated brain microenvironment supports tumor growth

A) Experimental design. B) Whole brain scans of sections from mice pre-treated with the indicated dose of radiation prior to injection with glioma cells and development of tumor. Tumor-bearing brains stained for CD34 to identify vasculature. C) Examples of CD34

immunofluorescence marking microvascular proliferation in mouse gliomas from mice pre-treated with the indicated dose of radiation. D) Quantification of microvascular proliferation in mice pre-treated with 0 Gy or 10 Gy radiation. E) Examples of Ki67 (magenta) staining of tumors from mice pre-treated with the indicated dose of radiation and F) quantification of Ki67 relative to DAPI in those tumors. Dots represent results from individual mice. D-F) Bars represent average from n=8 0 Gy control mice and n=6 10 Gy irradiated mice. Error bars are standard error of the mean. * P ≤ 0.05, unpaired t-test. G) Example of immunofluorescent staining of CD34 (red), glioma cells (Olig2, magenta), and the astrocyte marker GFAP (green). DAPI stains indicate nuclei (blue). White arrow indicates locations of interaction between astrocytes and vasculature.

Figure 3. Irradiated astrocytes produce a modified extracellular matrix which supports glioma cell stemness and radiation resistance

A) Experimental design showing two pathways for examining the effect of either astrocyte-derived soluble proteins or insoluble matrix proteins on glioma cells: Generation of astrocyte derived matrix (ADM) from control or irradiated astrocytes (ADMc and ADMi respectively); or suspension in sodium alginate to produce conditioned medium. B) Scatter plot showing percent SP of PIGPC cultured on ADMc or ADMi from n=3 experiments and sample plots showing an example of gating for SP. Error bars are SEM. ** P ≤ 0.01, unpaired t-test. D) Scatter plot showing SP of U3082 glioma cells cultured on ADMc or ADMi in serum-free conditions from n=4 experiments and sample plots showing an example of gating for SP. Error bars are SEM. ** P ≤ 0.01, ratio paired t-test. D) Self renewal of U3082 glioma cells pre-conditioned on ADMc or ADMi. Quantification of primary spheres (center) and secondary spheres (right) from n=3 experiments with images of sample secondary spheres from the indicated pre-conditioning (left).

Error bars are SEM, * P ≤ 0.05, unpaired t-test. E) Clonal survival of U251 glioma cells plated on ADMc or ADMi in triplicate wells, followed by irradiation with 0 Gy or 4 Gy. Scatter plot indicates percent survival from n=3 independent experiments and example colonies are shown below. Error bars are SEM. * P ≤ 0.05, unpaired t-test. F) Sample of most altered gene sets in U3082 cells cultured on ADMi compared to ADMc. NES indicates change in the enrichment score of cells cultured on ADMi relative to ADMc.

Figure 4. Irradiation induces a reactive astrocyte phenotype which persists within the original tumor volume after irradiation

A) Experimental design. B-C) Sections of brains from Nestin-*tv-a* mice injected with RCAS-*PDGFB* and treated upon symptoms with either B) 0 Gy radiation or C) 10 Gy radiation. Immunofluorescent detection of astrocytes with GFAP (red) and tumor with Olig2 (green) in whole brain scans and high magnification details from the tumor region of mouse brain sections are presented. Nuclei are stained with DAPI (blue). White outline in B indicates Olig2-positive tumor area. White line in C indicates probable tumor location before irradiation based on site of injection and GFAP-positivity. D) Quantification of GFAP relative to Olig2 measured in B (0 Gy) within Olig2-positive tumor area or C (10 Gy) within area of retained GFAP positivity. White line in C indicates example of boundary where GFAP to Olig2 ratio was measured. Scatter plot of n=3 mice from each treatment. Error bar are SEM. * P ≤ 0.05, unpaired t-test. E) Immunofluorescent detection of GFAP in astrocytes in culture 24 h after either 0 Gy or 10 Gy radiation and quantification of astrocyte body size in n=3 independent experiments, * P ≤ 0.05 unpaired t-test. F) Immunofluorescent detection of vimentin in astrocytes in culture 24 h after 0 Gy or 10 Gy irradiation and quantification of fluorescence intensity normalized to number of nuclei in image

from n=3 independent experiments * P ≤ 0.05, ratio paired t-test. Error bars are SEM. G-H) Quantification by ELISA of G) IL-6 and H) IL-8 in conditioned medium from cultured primary astrocytes the indicated time after treatment with 0 Gy or 10 Gy radiation. Averages from n=3 independent experiments. Error bars SEM. * P ≤ 0.05, ** P ≤ 0.01, unpaired t-test. ELISA results were normalized to total protein. Scatter plots represent values relative to the respective time point control. I) Heatmap of RNA sequencing results of astrocytes 24 h after irradiation with 0 Gy or 10 Gy. J) Kaplan-Meier curve showing survival of glioma patients with either high (blue) or low (red) expression of genes expressed by irradiated astrocytes.

Figure 5. Irradiated astrocytes secrete TGM2 *in vitro* and *in vivo* after irradiation

A) Mass spectrometry results of proteins detected in ADMi relative to ADMc. Matrix proteins with the largest and most significant increase or decrease in ADMi relative to ADMc. B) Western blot confirmation of increased expression of TGM2 in ADMi relative to ADMc. Quantification from n=6 independent samples of matrix proteins from control (ADMc) or irradiated (ADMi) astrocytes. Error bars are SEM. * P ≤ 0.05 by ratio paired t-test. C-G) Sections of brains from Nestin-*tv-a* mice injected with RCAS-*PDGFB* and treated upon symptoms with either C) 0 Gy radiation or D) 10 Gy radiation. Immunofluorescent detection with Olig2 (green, tumor), TGM2 (yellow), and GFAP (magenta, astrocytes) in whole brain scans and high magnification details of mouse brain sections are presented. Nuclei are stained with DAPI (blue). White outline in C indicates Olig2-positive tumor area. White line in D indicates probable tumor location before irradiation based on site of injection and TGM2-positivity. E) Quantification of percent area covered by TGM2 within the non-irradiated Olig2-positive tumor area (white outline in C) or within the area of retained TGM2 positivity in the irradiated tumors. White line in D indicates

example of boundary where TGM2 was measured. Scatter plot represents n=3 mice from each treatment. Error bars are SEM. * P ≤ 0.05, unpaired t-test. F) Quantification of TGM2 relative to Olig2 measured in C (0 Gy) within Olig2-positive tumor area or D (10 Gy) within area of retained TGM2 positivity. White line in D indicates example of boundary where TGM2 to Olig2 ratio was measured. Scatter plot represents n=3 mice from 0 Gy and n=4 mice from 10 Gy treatment. Error bars are SEM. * P ≤ 0.05, unpaired t-test. G) Example of CD34-labeled blood vessels (red) co-stained with TGM2 (yellow) with high magnification inset.

Figure 6. Astrocyte-derived TGM2 promotes glioma stemness after irradiation

A) Quantification of n=7 independent assays in which PIGPC glioma cells were cultured on ADMc or ADMi coated with vehicle or 32 mU TGM2 (left). Sample FACS plots with gating (right) * P ≤ 0.05, one-way ANOVA with Dunnet's multiple comparison's post-test. B) Quantification of n=4 independent assays in which PIGPC glioma cells were cultured on ADMc or ADMi with 0.5 μM of the TGM2 inhibitor GK921 (left). Sample FACs plots with gating (right). C) Quantification of n=3 independent assays in which PIGPC glioma cells were cultured on ADMc or ADMi with 100 μM of the TGM2 inhibitor dansylcadaverine (DC) (left). Sample FACS plots with gating (right). D) Clonal survival of U251 glioma cells plated on ADMc or ADMi in triplicate wells in media containing 0.1 μM GK921, followed by irradiation with 0 Gy or 5 Gy. Scatter plot indicates average percent survival from three independent experiments (left) and example colonies are shown on the right. Error bars are SEM. * P ≤ 0.05, unpaired t-test. E) Quantification of percent area covered by CD44 within the non-irradiated Olig2-positive tumor area or within the area of retained CD44 positivity in the irradiated tumors. (Boundaries indicated in Figures 4 C and D by white line.) Scatter plot represents n=3 mice from 0 Gy and n=4 mice from 10 Gy treatment. Error

bars are SEM. ** $P \leq 0.01$, unpaired t-test. F) Quantification of CD44 relative to Olig2 measured

in G (0 Gy) within Olig2-positive tumor area or H (10 Gy) within area of retained TGM2 positivity.

(Boundaries indicated in Figures 4 C and D by white line.) Scatter plot represents n=3 mice from

0 Gy and n=4 mice from 10 Gy treatment. Error bars are SEM. * $P \leq 0.05$, unpaired t-test.

Figure 7. TGM2 is a potential therapeutic target in GBM

A-B) Immunofluorescent detection of Olig2 (yellow) or nuclei (DAPI, blue) in cryosections of

organotypic brain slices from mice bearing gliomas. Brain slices were treated with either A) 0 μM

or B) 5 μM of the TGM2 inhibitor GK921. C) Quantification percent of nuclei positive for Olig2

in organotypic brain slices from four mice. D) TGM2 transcript expression in glioma grades II,

III, and IV. E) TGM2 transcript expression in IDH mutant (IDHmut) glioma with or without

1p/19q codeletion (codel and non-codel respectively) or IDHwt glioma. F) Kaplan-Meier curve

showing survival of glioma patients with either high (red) or low (blue) TGM2 expression. G)

Kaplan-Meier curve showing survival of GBM patients with IDHwt tumors with TGM2 transcript

expression in either the upper 10% (red) or lower 90% (blue). H) Proposed model of stimulation

of TGM2 release from astrocytes after irradiation and its role in survival of tumor cells. Grey

cells, glioma cells that respond to radiotherapy. Red cells, glioma cells that survive radiotherapy.

Purple cells, astrocytes.